Nonlinear Modeling and Control Design of Active Helicopter Blades

Matthias Althoff

Postdoctoral Researcher,

Carnegie Mellon University,

Pittsburgh, PA

Mayuresh J. Patil

Associate Professor,

Virginia Polytechnic Institute and State University,

Blacksburg, VA

Johannes P. Traugott

Research Assistant,

Technische Universität München,

Munich, Germany

Abstract

This paper presents the theoretical basis for the simulation and control of active helicopter blades. The analysis is based on a model that considers the structural dynamics, the aerodynamics, as well as the integrated blade actuation and sensing. The effect of the integral actuation enters the beam model via an active beam cross-sectional analysis. A 2-D incompressible, inviscid, quasi-steady aerodynamic model is coupled to the active structural model. For simulation, analysis, and control design, the blade model is discretized in space using a Galerkin approach. The resulting nonlinear

Work has been presented at the 47th Structures, Structural Dynamics & Materials Conference, Newport, Rhode Island, May 2006.

model of high order is reduced using the aeroelastic modes of the blade. Finally, the usefulness of a reduced order model is demonstrated by designing an energy optimal linear-quadratic-Gaussian control.

Nomenclature

B_i	axes of the deformed beam
b_i	axes of the undeformed beam
F	internal force
f	external force
H	angular momentum
J	cost function
K	state feedback controller gain
M	internal moment
m	external moment
P	linear momentum
P^{act}	power due to active elements
P^{bou}	power due to forces at the boundaries
P^{ext}	power due to external loads
q	time function
T	kinetic energy
$\mathbf{T}$	transformation matrix
t	time
U	potential energy
u	voltage
V	linear velocity
x	beam reference line
$\bar{x}$	normalized beam reference line

γ	strain
κ	curvature
Ω	angular velocity

Typefaces

$\mathcal{A}, \mathcal{B}, \mathcal{C}, \ldots$	full order beam
$\mathbf{A}, \mathbf{B}, \mathbf{C}, \ldots$	reduced order beam
$\mathrm{A}, \mathrm{B}, \mathrm{C}, \ldots$	beam in state space form
$\square'$	derivative with respect to the beam reference line x
$\dot{\square}$	absolute time derivative
$\square^0$	steady state
$\square^{\mathbb{0}}$	exact boundary condition value at $x = \mathbb{0}$
$\square^{\mathbb{L}}$	exact boundary condition value at $x = \mathbb{L}$
$\Phi^{\square}$	assumed mode of $\square$

Introduction

Active structures have the potential to outperform conventional structures in many ways. In the case of helicopter blades, active structures can overcome the compromise between vibration and weight reduction (Refs. 1, 2). This potential has been investigated in tests of the Active Twist Rotor (ATR) blade, whose parameters are the basis for the theoretical results presented herein. The present paper is a continuation of the research presented in Traugott et al. in Ref. 3 dealing with the nonlinear dynamic solution and control design of active helicopter blades. The significant new developments are:

- A structural dynamic model is used based on a nonlinear Galerkin approach which is more efficient as compared to the finite element method (FEM) (Ref. 4). For example, in the linearized perturbation analysis it is shown that using 10 modes for the Galerkin approach and 10 nodes for the FEM approach (both 120 states), the 3^{rd} bending mode frequency is accurate up to three significant digits using the Galerkin approach while the FEM approach has an error of 10%.

- A quasi-steady aerodynamic model is included.
- A nonlinear model order reduction technique is used to derive a low-order, high fidelity nonlinear blade model for control design.
- Nonlinear control design is investigated.

The paper is organized as follows. First, the blade model is introduced followed by the Galerkin approach for spatial discretization. Modal analysis is presented next and the obtained normal modes are utilized for model order reduction. Finally, the control design is discussed based on the reduced order model.

Blade Model

Accurate modeling of active helicopter blade dynamics requires to combine physical models of different domains. The four models which need to be developed and integrated are: the structural dynamic model, the aerodynamic model, the actuation model and the sensing model of the helicopter blade. The structural and aerodynamic models are inherently nonlinear. The presented models are an extension of earlier work of the authors in Refs. 4, 5.

Structural model

In order to compute the dynamics of the helicopter blade at low computational costs, a nonlinear beam model developed by Hodges is used (Refs. 6, 7). This model takes advantage of the one-dimensional characteristics of a helicopter blade undergoing large deformation and small strain and is a better choice compared to 3-D finite-element analysis (Ref. 8). The beam formulation is intrinsic, i.e. neither displacement nor rotation variables appear in the beam equations. The intrinsic formulation is very compact and furthermore applicable for general beams (anisotropic, non-uniform, twisted and curved).

The beam model is composed of vector equations in terms of vector variables. The measure numbers (or scalar components) of the vector variables in the deformed frame (B-frame) are used. The B-frame is orthogonal and defined by the cross section of the deformed beam as seen in Fig. 1. The B_2-axis and the B_3-axis lie in the cross-section with the B_1-axis defined by $B_1 = B_2 \times B_3$. Note that in this work, all

variables are written in the B-frame of the deformed beam.

The intrinsic equations for the nonlinear dynamics of the beam are:

$$\begin{aligned} F' + (\tilde{\mathbb{k}} + \tilde{\kappa})F + f^{aero} + f^{dist} &= \dot{P} + \tilde{\Omega}P, \\ M' + (\tilde{\mathbb{k}} + \tilde{\kappa})M + (\tilde{e}_1 + \tilde{\gamma})F + m^{aero} + m^{dist} &= \dot{H} + \tilde{\Omega}H + \tilde{V}P, \\ V' + (\tilde{\mathbb{k}} + \tilde{\kappa})V + (\tilde{e}_1 + \tilde{\gamma})\Omega &= \dot{\gamma}, \\ \Omega' + (\tilde{\mathbb{k}} + \tilde{\kappa})\Omega &= \dot{\kappa}, \end{aligned} \tag{1}$$

where $(\ )'$ denotes the derivative with respect to the beam reference line and $\dot{(\ )}$ denotes the absolute time derivative. F and M are the measure numbers of the internal force and moment vector (generalized forces), P and H are the measure numbers of the linear and angular momentum vector (generalized momenta), γ and κ are the beam strains and curvatures (generalized strains), V and Ω are the linear and angular velocity measure numbers (generalized velocities). The external forces and moments due to aerodynamic effects are f^{aero}, m^{aero} and due to disturbances are f^{dist}, m^{dist} respectively. $\mathbb{k} = [\mathbb{k}_1 \ \ \mathbb{k}_2 \ \ \mathbb{k}_3]$ is the initial twist/curvature of the beam and $e_1 = [1 \ \ 0 \ \ 0]^T$. The tilde operator transforms a vector a to a matrix $\widetilde{a}$ so as to affect a cross product when left-multiplied to the vector b, i.e., $\widetilde{a}b = a \times b$.

The intrinsic beam equations provide 4 vector equations for 8 vector unknowns (F, M, P, H, γ, κ, V, Ω). In order to complete a solvable set of equations, 4 more vector equations are needed. Two equations relate the generalized forces (F, M) and the generalized strains (γ, κ) via the beam cross-section stiffness matrix. The beam cross-section inertia matrix leads to the relation between the generalized momenta (P, H) and the generalized velocities (V, Ω). Both relations are the constitutive equations for an active beam and are derived from an accurate cross-sectional analysis using the theory of Patil and Johnson in Ref. 9 (for thin-walled beams) or Cesnik and Palacios in Ref. 10 (for general configuration):

$$\begin{aligned} \begin{Bmatrix} F \\ M \end{Bmatrix} &= \begin{bmatrix} \mathbb{R} & \mathbb{S} \\ \mathbb{S}^T & \mathbb{T} \end{bmatrix}^{-1} \begin{Bmatrix} \gamma \\ \kappa \end{Bmatrix} - \begin{Bmatrix} F^A \\ M^A \end{Bmatrix}, \\ \begin{Bmatrix} P \\ H \end{Bmatrix} &= \begin{bmatrix} \mathbb{G} & \mathbb{K} \\ \mathbb{K}^T & \mathbb{I} \end{bmatrix} \begin{Bmatrix} V \\ \Omega \end{Bmatrix}, \end{aligned} \tag{2}$$

where $\mathbb{R}$, $\mathbb{S}$ and $\mathbb{T}$ are the cross-sectional flexibilities, and F^A, M^A are generalized forces induced by the

active elements. The inertia matrices have the following components:

$$\mathbb{G} = \mu I = \begin{bmatrix} \mu & 0 & 0 \\ 0 & \mu & 0 \\ 0 & 0 & \mu \end{bmatrix}, \qquad \mathbb{K} = -\mu\tilde{\xi} = \begin{bmatrix} 0 & \mu\tilde{\xi}_3 & -\mu\tilde{\xi}_2 \\ -\mu\tilde{\xi}_3 & 0 & 0 \\ \mu\tilde{\xi}_2 & 0 & 0 \end{bmatrix}, \qquad \mathbb{I} = \begin{bmatrix} \mathbb{i}_2 + \mathbb{i}_3 & 0 & 0 \\ 0 & \mathbb{i}_2 & \mathbb{i}_{23} \\ 0 & \mathbb{i}_{23} & \mathbb{i}_3 \end{bmatrix}, \tag{3}$$

where μ, ξ, $\mathbb{i}_2$, $\mathbb{i}_3$, $\mathbb{i}_{23}$ are the mass per unit length, mass center offset and the three cross-sectional mass momenta of inertia per unit length.

Aerodynamic model

To take into account the primary aeroelastic effects, an incompressible, inviscid, quasi-steady, 2-D aerodynamic model from Ref. 5 based on a finite-state airload model in Ref. 11 is used. The model neglects the unsteady effects due to the wake. The aerodynamic loads f^{aero} and m^{aero} in Eq. (1) are calculated using:

$$\begin{aligned} f^{aero} &= \begin{Bmatrix} 0 \\ -\rho b C_{l0} \check{V}_2 \check{V}_3 + \rho b C_{l\alpha} \check{V}_3^2 - \rho b C_{d0} \check{V}_2^2 \\ \rho b C_{l0} \check{V}_2^2 - \rho b (C_{l\alpha} + C_{d0}) \check{V}_2 \check{V}_3 + \frac{1}{2} \rho b^2 C_{l\alpha} \check{V}_2 \Omega_1 \end{Bmatrix}, \\ \check{\check{m}}^{aero} &= \begin{Bmatrix} 2\rho b^2 C_{m0} \check{V}_2^2 - \frac{1}{4} \rho b^3 C_{l\alpha} \check{V}_2 \Omega_1 \\ 0 \\ 0 \end{Bmatrix}, \end{aligned} \tag{4}$$

where $\check{(\,)}$ denotes a variable measured at mid-chord and $\check{\check{(\,)}}$ denotes a variable calculated at quarter-chord. The parameter ρ is the air density and b is the semi-chord. Moreover, one can see from Fig. 2 that:

$$\begin{aligned} \check{V}_3 = V_3 - \xi b \Omega_1, \quad \check{V}_2 = V_2, \\ m_1^{aero} = \check{\check{m}}_1^{aero} + (0.5 - \xi) b f_3^{aero}. \end{aligned} \tag{5}$$

After inserting Eq. (5) into Eq. (4), the new equations can be written in terms of V and Ω as:

$$\begin{aligned} f^{aero} &= \begin{Bmatrix} 0 & 1 & 0 \end{Bmatrix}^T \left[V^T \mathbb{X}^{VV} V + V^T \mathbb{X}^{V\Omega} \Omega + \Omega^T \mathbb{X}^{\Omega\Omega} \Omega \right] + \begin{Bmatrix} 0 & 0 & 1 \end{Bmatrix}^T \left[V^T \mathbb{Y}^{VV} V + V^T \mathbb{Y}^{V\Omega} \Omega \right], \\ m^{aero} &= \begin{Bmatrix} 1 & 0 & 0 \end{Bmatrix}^T \left[V^T \mathbb{Z}^{VV} V + V^T \mathbb{Z}^{V\Omega} \Omega \right], \end{aligned} \tag{6}$$

where the matrices used above are defined as:

$$
\begin{aligned}
\mathbb{Y}^{VV} &= \rho b \begin{bmatrix} 0 & 0 & 0 \\ 0 & C_{l0} & -(C_{l\alpha}+C_{d0}) \\ 0 & 0 & 0 \end{bmatrix}, & \mathbb{X}^{VV} &= \rho b \begin{bmatrix} 0 & 0 & 0 \\ 0 & -C_{d0} & -C_{l0} \\ 0 & 0 & C_{l\alpha} \end{bmatrix}, \\
\mathbb{Y}^{V\Omega} &= \rho b^2 \begin{bmatrix} 0 & 0 & 0 \\ (0.5+\xi)C_{l\alpha}+\xi C_{d0} & 0 & 0 \\ 0 & 0 & 0 \end{bmatrix}, & \mathbb{X}^{V\Omega} &= \xi\rho b^2 \begin{bmatrix} 0 & 0 & 0 \\ C_{l0} & 0 & 0 \\ -2C_{l\alpha} & 0 & 0 \end{bmatrix}, \\
\mathbb{Z}^{VV} &= \rho b^2 \begin{bmatrix} 0 & 0 & 0 \\ 0 & 2C_{m0}+(0.5-\xi)C_{l0} & -(0.5-\xi)(C_{l\alpha}+C_{d0}) \\ 0 & 0 & 0 \end{bmatrix}, & \mathbb{X}^{\Omega\Omega} &= \xi^2\rho b^3 \begin{bmatrix} C_{l\alpha} & 0 & 0 \\ 0 & 0 & 0 \\ 0 & 0 & 0 \end{bmatrix}, \\
\mathbb{Z}^{V\Omega} &= \xi\rho b^3 \begin{bmatrix} 0 & 0 & 0 \\ -\xi C_{l\alpha}+(0.5-\xi)C_{d0} & 0 & 0 \\ 0 & 0 & 0 \end{bmatrix}.
\end{aligned}
\tag{7}
$$

Actuation model

The actuation in an active helicopter blade like the Active Twist Rotor (ATR) is provided by active fiber composites (AFC) that are distributed as discrete segments over the span of the blade (see Fig. 3). Each segment may contain multiple layers of AFCs which can be controlled independently (ATR contains four) and induce constant generalized forces F^A and M^A in the blade structure (see Eq. (2)). The generalized active forces are linearly related to the applied voltages as

$$
\begin{Bmatrix} F_u^A \\ M_u^A \end{Bmatrix} = \begin{bmatrix} \mathbb{R} & \mathbb{S} \\ \mathbb{S}^T & \mathbb{T} \end{bmatrix}^{-1} \begin{bmatrix} \mathbb{E} \\ \mathbb{F} \end{bmatrix} u_u, \tag{8}
$$

where u_u is the applied voltage vector for one blade segment consisting of multiple voltages. $\mathbb{E}$ and $\mathbb{F}$ are constants relating the applied voltage to the active generalized strains which are transformed to the active generalized forces via the cross-section stiffness matrix. The cross-sectional flexibilities $\mathbb{R}$, $\mathbb{S}$, and $\mathbb{T}$ are as defined in Eq. (2).

Sensing model

The helicopter blade is assumed to be equipped with a number of equidistantly distributed sensors which measure the generalized strains γ and κ along the blade reference line. The results presented in the later sections assume five sensor locations $x = \frac{y-1}{4}\mathbb{L}$, where $y = 1 \ldots 5$ refers to the y^{th} sensor location and $\mathbb{L}$ is the blade length. Furthermore, the sensors are assumed to relate the generalized strains linearly to the voltage outputs as

$$y_y = \begin{bmatrix} \mathbb{O} & \mathbb{P} \end{bmatrix} \begin{Bmatrix} \gamma(x = \frac{y-1}{4}\mathbb{L}) \\ \kappa(x = \frac{y-1}{4}\mathbb{L}) \end{Bmatrix}, \tag{9}$$

where y_y denotes the measured voltages. $\mathbb{O}$ and $\mathbb{P}$ relate the sensed voltages to the generalized strains γ and κ. Without loss of generality, the sensor matrices are simplified to $\mathbb{O} = I$ and $\mathbb{P} = I$, where $I \in \mathbb{R}^{3\times3}$ is the identity matrix.

Galerkin Discretization

The helicopter blade model equations (Eqs. (1), (2), (6), (8), (9)) form a solvable set with V, Ω, κ and γ as unknowns. For simulation and analysis purposes, this equation set is discretized with respect to space. Unlike the most common approaches based on the finite element method, the helicopter blade model is discretized using a Galerkin approach (Ref. 12). By using special weighting functions in the Galerkin approach presented here, the approximated solution fulfills the law of energy conservation if no active elements are modeled (Ref. 4). If active elements are used, the law of energy conservation can be fulfilled approximately. Additionally, the boundary conditions of the problem are satisfied weakly in the Galerkin approach.

Brief introduction to Galerkin discretization

For readers who are not familiar with the Galerkin approach, a brief introduction is presented in this subsection. Consider a partial differential equation in terms of the variable w(x,t) given by:

$$f\left(w(x,t),\, \dot{w}(x,t),\, w'(x,t),\, x,\, t\right) = 0$$

The solution can be approximated by a separation of variables in space and time as

$$w(x,t) = \sum_{i=1}^{n} \Phi_i(x) q_i(t),$$

such that the partial differential equations can be approximated as

$$f\left(\Phi_i(x),\, \Phi_i'(x),\, q_i(t),\, \dot{q}_i(t),\, x,\, t\right) \approx 0. \tag{10}$$

The right relation in Eq. (10) is not equal to zero in general. Now, it is required that for each weighting function $\Psi_k(x)$, $k \in \mathbb{N}$, the integral of Eq. (10) weighted by $\Psi_k(x)$ has to be zero.

$$\int_0^L \left\{\Psi_k(x)\, f\left(\Phi_i(x), \Phi_i'(x), q_i(t), \dot{q}_i(t), x, t\right)\right\} dx = 0; \tag{11}$$

The final equations (Eq. (11)) are only ordinary differential equations in time as the integral eliminates the space dependent part. If $k, i \to \infty$, the Galerkin approximation solves the original partial differential equation exactly. The Φ_i are called *assumed modes*, the Ψ_k are *weighting functions* and the q_i are *time functions*.

Energy optimal weighting

In this subsection, the physical interpretation for a special choice of weighting functions for the Galerkin discretization of the blade model is given. Without loss of generality, the beam is assumed to be cantilevered and thus the boundary conditions of the blade are chosen to constrain the generalized velocities at the root ($x = \mathbb{0}$) and the generalized forces at the tip ($x = \mathbb{L}$) of the beam. The boundary conditions can be written as:

$$V(\mathbb{0}) = V^{\mathbb{0}}, \quad \Omega(\mathbb{0}) = \Omega^{\mathbb{0}}, \quad F(\mathbb{L}) = F^{\mathbb{L}}, \quad M(\mathbb{L}) = M^{\mathbb{L}}. \tag{12}$$

Consider the following weighted sum of all the differential equations from Eq. (1) and the boundary conditions from Eq. (12):

$$
\begin{aligned}
0 = \int_{\mathbb{0}}^{\mathbb{L}} \Big\{ & \\
& V^T \left[\dot{P} + \widetilde{\Omega} P - F' - (\widetilde{\mathbb{k}} + \widetilde{\kappa}) F - f\right] \\
& + \Omega^T \left[\dot{H} + \widetilde{\Omega} H + \widetilde{V} P - M' - (\widetilde{\mathbb{k}} + \widetilde{\kappa}) M - (\widetilde{e_1} + \widetilde{\gamma}) F - m\right] \\
& + \left(F + F^A\right)^T \left[\dot{\gamma} - V' - (\widetilde{\mathbb{k}} + \widetilde{\kappa}) V - (\widetilde{e_1} + \widetilde{\gamma}) \Omega\right] \\
& + \left(M + M^A\right)^T \left[\dot{\kappa} - \Omega' - (\widetilde{\mathbb{k}} + \widetilde{\kappa}) \Omega\right] \\
& \Big\} dx \\
- \left(F(\mathbb{0}) + F^A(\mathbb{0})\right)^T & \left[V(\mathbb{0}) - V^{\mathbb{0}}\right] - \left(M(\mathbb{0}) + M^A(\mathbb{0})\right)^T \left[\Omega(\mathbb{0}) - \Omega^{\mathbb{0}}\right] \\
& + V(\mathbb{L})^T \left[F(\mathbb{L}) - F^{\mathbb{L}}\right] \qquad + \Omega(\mathbb{L})^T \left[M(\mathbb{L}) - M^{\mathbb{L}}\right],
\end{aligned}
\tag{13}
$$

where $V^{\mathbb{0}}$ and $\Omega^{\mathbb{0}}$ are the exact linear and angular velocities at the root, while $F^{\mathbb{L}}$ and $M^{\mathbb{L}}$ are the force and moment at the tip. Note that the external forces due to aerodynamic effects and disturbances in Eq. (13) are summarized as f and m for simplicity reasons. After integrating by parts and simplifying Eq. (13) we have

$$
\dot{T} + \dot{U} = P^{ext} + P^{bou} + P^{act*}, \tag{14}
$$

where the variables are defined in Table 1. Equation (14) states the law of energy conservation if $P^{act*} = 0$ (passive beam). For active beams P^{act*} approximates the power P^{act} generated by the active elements as:

$$
P^{act*} = \int_0^L \Big\{ F^{A^T} \underbrace{\left[V' + (\widetilde{\mathbb{k}} + \widetilde{\kappa}) V + (\widetilde{e_1} + \widetilde{\gamma}) \Omega\right]}_{\approx \dot{\gamma}, \text{ see Eq. (1)}} + M^{A^T} \underbrace{\left[\Omega' + (\widetilde{\mathbb{k}} + \widetilde{\kappa}) \Omega\right]}_{\approx \dot{\kappa}, \text{ see Eq. (1)}} \Big\} dx + F^{A^T} \underbrace{\left[V(\mathbb{0}) - V^{\mathbb{0}}\right]}_{\approx 0} + M^{A^T} \underbrace{\left[\Omega(\mathbb{0}) - \Omega^{\mathbb{0}}\right]}_{\approx 0} \tag{15}
$$

Thus, the weighting presented in Eq. (13) leads to an approximate energy balance for the active beam. The error of the energy balance in Eq. (14) is caused by the active elements only. If weighting functions other than those presented in Eq. (13) are used, there will be error in the energy balance caused by all values of Table 1. For this reason, the weighting functions used in this work provide the best known solution in terms of energy conservation.

Assumed modes and weighting functions

The unknown variables of the Galerkin discretization are approximated according to Table 2 using an expansion of products of known spatial functions (assumed modes) and unknown temporal functions (generalized coordinates). Note that a mixed matrix/tensor notation is used (the dimensions are given in the last row in the left column of Table 2) and all variables have a common time function $q(t)$. The advantage of the common time function is that the complete discretized blade model can be written in a single equation.

The weighting functions for the Galerkin approach are basically chosen as shown in Eq. (13). Thus, the set of weighing functions are the same as the set of variables. After substituting for the weighting functions in terms of the expansions, we get a single equation, but since each generalized coordinate is arbitrary, this leads to multiple equations for each set of weighing functions. Hence, multiple equations are obtained by the Galerkin integral by using each set of weighting functions, e.g. the weighting function $V(x,t)$ is replaced by several assumed modes $\Phi_l^V(x)$.

In this work, the assumed modes for each variable and each direction are chosen identically. Due to numerical performance, orthogonal shifted Legendre functions from (Ref. 13, pp. 332–357) have been used.

$$\bar{V}_l(\bar{x}) = \bar{\Omega}_l(\bar{x}) = \bar{\gamma}_l(\bar{x}) = \bar{\kappa}_l(\bar{x}) = I\tilde{P}_l(\bar{x}), \tag{16}$$

where I is a 3×3 identity matrix, $\bar{x}$ is the normed coordinate of the beam reference line ($\bar{x} = \frac{x}{\mathbb{L}}$), and $\tilde{P}_l()$ are the shifted Legendre functions. After applying the Galerkin approach to Eq. (13) and discretizing the measurement equation, the beam model has the following form written in matrix/tensor notation:

$$\begin{aligned} \mathcal{A}_{ki}\dot{q}_i + \mathcal{B}_{ki}q_i + \mathcal{C}_{kij}q_iq_j + \mathcal{D}_k + \mathcal{E}_{ku}u_u + \mathcal{F}_{kiu}q_iu_u + f_k + m_k = 0, \\ y_y = \mathcal{M}_{yi}q_i, \end{aligned} \tag{17}$$

where

$$\mathcal{B}_{ki} = \mathcal{B}_{ki}^{no\,BC} + \mathcal{B}_{ki}^{BC}, \quad \mathcal{C}_{kij} = \mathcal{C}_{kij}^{struc} + \mathcal{C}_{kij}^{aero}, \quad \mathcal{D}_k = \mathcal{D}_k^{BC}, \quad \mathcal{E}_{ku} = \mathcal{E}_{ku}^{no\,BC} + \mathcal{E}_{ku}^{BC}. \tag{18}$$

The expressions for the tensors in Eqs. (17) and (18) are given in the appendix.

Modal Analysis

In order to get an insight into the behavior of the helicopter blade, the steady state, natural frequencies and natural modes (free vibration modes) are calculated for parameter values specified in Table 4. The steady state solution q_i^0 of the helicopter blade has been computed for the boundary conditions specified in Eq. (12) with $V^{\mathbb{0}} = [0 \quad 0 \quad 0]^T$ m/s, $F^{\mathbb{L}} = [0 \quad 0 \quad 0]^T$ N, $M^{\mathbb{L}} = [0 \quad 0 \quad 0]^T$ Nm, $\Omega^{\mathbb{0}} = [0 \quad 0 \quad 72]^T$ rad/s. The solution has been obtained reliably using the Newton-Raphson algorithm and is presented in Fig. 4 over the beam reference line x varying from 0 to $\mathbb{L} = 1.397$ [m]. The natural frequencies and modes are obtained from the unforced linearized blade model given by

$$\hat{\mathcal{A}}_{ki}\dot{q}_i + \hat{\mathcal{B}}_{ki}q_i = 0, \tag{19}$$

where

$$\hat{\mathcal{A}}_{ki} = \mathcal{A}_{ki}, \quad \hat{\mathcal{B}}_{ki} = \mathcal{B}_{ki} + (\mathcal{C}_{kij} + \mathcal{C}_{kji})\, q_j^0 + \mathcal{F}_{kiu}u_u^0. \tag{20}$$

The free vibration solution (fvs) of Eq. (19) is:

$$q_i^{fvs}(t) = c_l n_{il} e^{\lambda_l t} + \hat{c}_l \hat{n}_{il} e^{\hat{\lambda}_l t} = \mathbf{T}_{il} \left\{ e^{\lambda_l t} \; e^{\hat{\lambda}_l t} \right\}^T, \tag{21}$$

where $\hat{()}$ denotes conjugate complex values, c_l and $\hat{c}_l$ are the constant which can be calculated using the initial conditions, n_{il} and $\hat{n}_{il}$ are the eigenvectors, λ_l and $\hat{\lambda}_l$ denote the eigenvalues of Eq. (19), and $\mathbf{T}_{il} = [c_l n_{il} \quad \hat{c}_l \hat{n}_{il}]$. Inserting Eq. (21) into Table 2 yields the natural modes of V, Ω, γ and κ given in Table 3. Note that the calculations can be performed in terms of real variables by considering the real and imaginary parts of the set of complex conjugate eigenvectors (Ref. 14). The natural frequencies of the helicopter blade are presented in Table 5 and are compared to results from the simulation tool NATASHA (Ref. 5) and the purely structural model (no aerodynamics). For the aeroelastic and the structural model, 20 Legendre functions have been used. The NATASHA results are based on 50 beam finite elements. Firstly, the aeroelastic simulation theory presented in the paper is validated by comparing to the results generated by NATASHA. Secondly, one can see that the aerodynamics is mainly adding damping and reducing the frequency of the 1^{st} bending mode. The dominant natural modes are shown in Fig. 5.

Model Reduction

The discretization results in a model (Eq. (17)) of high order depending on the number of assumed modes. As both, the accuracy and the computational costs of time marching simulations increase with the number of assumed modes, one has to choose a good compromise. A possibility to avoid such a compromise is to find assumed modes that capture the dynamics of the rotating blade more accurately as compared to Legendre functions. The model order reduction follows this approach by taking low number of relevant assumed modes to reduce the system order without loosing accuracy.

One choice of assumed modes that capture the linear dynamics are the natural modes of the system linearized at the steady state. Since these modes are used in the expansions applied to the complete nonlinear model, the primary nonlinear behavior is also captured. In order to improve the nonlinear prediction of the linear modes, perturbation modes as presented in Refs. 15, 16 have also been investigated. Although perturbation modes showed a better performance regarding to the tracking of natural frequencies, they can lead to errors in the blade damping for equations in the mixed form. For this reason, only natural modes are used for order reduction. Another advantage of the natural modes is that the resulting reduced model has the same, but less natural frequencies and modes at the linearization point. Furthermore, the steady state solution is included in the new approximation of the model variables. Thus, the quality of the steady state is not affected by the order reduction and the new steady state $\mathbf{q}_r^0$ is always zero, resulting into a simple linearized reduced system.

The new variable approximations are listed in Table 6. Substituting the new assumed modes into Eq. (17) yields

$$\begin{aligned} \mathbf{A}_{tr}\dot{\mathbf{q}}_r + \mathbf{B}_{tr}\mathbf{q}_r + \mathbf{C}_{trs}\mathbf{q}_r\mathbf{q}_s + \mathbf{E}_{tu}u_u + \mathbf{F}_{tru}\mathbf{q}_r u_u + \mathbf{T}_{kt}f_k + \mathbf{T}_{kt}m_k = 0, \\ y_y = \mathbf{M}_{yr}\mathbf{q}_r + y_y^0, \end{aligned} \tag{22}$$

where

$$\begin{aligned} \mathbf{A}_{tr} &= \mathcal{A}_{ki}\mathbf{T}_{kt}\mathbf{T}_{ir}, & \mathbf{B}_{tr} &= \left[\mathcal{B}_{ki} + (\mathcal{C}_{kij} + \mathcal{C}_{kji})q_j^0 + \mathcal{F}_{kiu}u_u^0\right]\mathbf{T}_{kt}\mathbf{T}_{ir}, \\ \mathbf{C}_{trs} &= \mathcal{C}_{kij}\mathbf{T}_{kt}\mathbf{T}_{ir}\mathbf{T}_{js}, & \mathbf{E}_{tu} &= \left[\mathcal{E}_{ku} + \mathcal{F}_{kiu}q_i^0\right]\mathbf{T}_{kt}, \\ \mathbf{F}_{tru} &= \mathcal{F}_{kiu}\mathbf{T}_{kt}\mathbf{T}_{ir}, & \mathbf{M}_{yr} &= \mathcal{M}_{yi}\mathbf{T}_{ir}, \\ y_y^0 &= \mathcal{M}_{yi}q_i^0, \end{aligned} \tag{23}$$

and $(\,)^0$ denotes the steady-state solution. Since the modal expansion calculates motion relative to the nonlinear steady state, the steady state solution of the transformed system is always $\mathbf{q}_r^0 = 0$. The reduced nonlinear system is the basis for low-order analysis as well as for control design. As $\mathbf{A}_{tr}$ is invertible, the state space formulation of Eq. (22) can be obtained by premultiplying the first equation in Eq. (22) with $\mathbf{A}_{tr}^{-1}$. The state space formulation is:

$$\begin{aligned} \dot{\mathbf{q}}_t &= \mathrm{B}_{tr}\mathbf{q}_r + \mathrm{C}_{trs}\mathbf{q}_r\mathbf{q}_s + \mathrm{E}_{tu}u_u + \mathrm{F}_{tru}\mathbf{q}_r u_u + \mathrm{G}_{kt}f_k + \mathrm{H}_{kt}m_k, \\ y_y &= \mathbf{M}_{yr}\mathbf{q}_r + y_y^0, \end{aligned} \tag{24}$$

where

$$\begin{aligned} \mathrm{B}_{tr} &= -\mathbf{A}_{th}^{-1}\mathbf{B}_{hr},\ \mathrm{C}_{trs} = -\mathbf{A}_{th}^{-1}\mathbf{C}_{hrs},\ \mathrm{E}_{tu} = -\mathbf{A}_{th}^{-1}\mathbf{E}_{hu}, \\ \mathrm{F}_{tru} &= -\mathbf{A}_{th}^{-1}\mathbf{F}_{hru},\ \mathrm{G}_{kt} = -\mathbf{A}_{kh}^{-1}\mathbf{T}_{ht},\ \ \mathrm{H}_{kt} = -\mathbf{A}_{kh}^{-1}\mathbf{T}_{ht}. \end{aligned} \tag{25}$$

Even if the model is reduced, from 240 to 12 states, the reduced model still shows good performance. Consider Fig. 6 where the natural modes of the full (240 states) and reduced (12 states) model are compared in two plots. The solid lines show the frequencies of the full and the dashed lines the frequencies of the reduced model. For the reduced order model the steady states are still computed using the full model, but the reduced order models are obtained by using a single set of modeshapes. In the left plot, the frequency variation is calculated under varying rotational speed Ω_3 and in the right one under varying external force f_3 (constant along reference line, rotation speed $\Omega_3^0 = 72$rad/s). One can see that the natural frequencies are not affected noticeably by a varying external force f_3 (f_3=50 N m^{-1} is the estimated force to lift the helicopter), whereas the rotation speed has a much larger effect. The reduced model is able to track the change in the frequency accurately.

Control Design

To illustrate the use of the model for control design, a linear optimal controller is designed. The control design takes advantage of the high fidelity and low order of the reduced blade model in Eq. (24). An energy optimal linear-quadratic-Gaussian (LQG) control design is performed, which is the combination of a Kalman filter and a linear-quadratic regulator (Ref. 17). In order to show the robustness of the controller, it is tested on a high fidelity model with twice as many states as the model used for the control design.

Cost function

The linear-quadratic-Gaussian (LQG) control is optimal in the sense that it minimizes the cost function

$$J = E\left\{\lim_{T\to\infty}\frac{1}{T}\int_0^T [\mathbf{q}\ u]^T W[\mathbf{q}\ u]dt\right\} \to min, \tag{26}$$

where $E\{\}$ is the expectation and W a weighting matrix. In this work, the state $\mathbf{q}$ and the input u are weighted separately, such that $[\mathbf{q}\ u]^T W[\mathbf{q}\ u] = \mathbf{q}^T Q\mathbf{q} + u^T Ru$, where Q weights the control error since $\mathbf{q} = 0$ is desired and R the control effort. Since the controller is not determined by the absolute values of the weighting matrices, but their relative values, R is chosen to be identity ($R = I$). The weight of the control error Q is chosen as

$$Q = \frac{1}{2}\alpha\int_0^L \mathbf{T}^T \begin{bmatrix}\Phi^V\\ \Phi^\Omega\\ \Phi^\gamma\\ \Phi^\kappa\end{bmatrix}^T \begin{bmatrix}\mathbb{G} & \mathbb{K} & 0 & 0\\ \mathbb{K}^T & \mathbb{I} & 0 & 0\\ 0 & 0 & \mathbb{U} & \mathbb{V}\\ 0 & 0 & \mathbb{V}^T & \mathbb{W}\end{bmatrix} \begin{bmatrix}\Phi^V\\ \Phi^\Omega\\ \Phi^\gamma\\ \Phi^\kappa\end{bmatrix} \mathbf{T}dx, \quad \begin{bmatrix}\mathbb{U} & \mathbb{V}\\ \mathbb{V}^T & \mathbb{W}\end{bmatrix} = \begin{bmatrix}\mathbb{R} & \mathbb{S}\\ \mathbb{S}^T & \mathbb{T}\end{bmatrix}^{-1}, \tag{27}$$

where the assumed modes are written in matrix notation, $\mathbb{G}$, $\mathbb{K}$, $\mathbb{I}$ are the inertia matrices from (2) and $\mathbb{U}$, $\mathbb{V}$, $\mathbb{W}$ are the cross-sectional stiffness matrices, which are related to the cross-sectional flexibilities $\mathbb{R}$, $\mathbb{S}$, $\mathbb{T}$ from (2) by the inversion presented above. After inserting Eq. (27) into $\mathbf{q}^T Q\mathbf{q}$ of Eq. (26) we obtain

$$\mathbf{q}^T Q\mathbf{q} \overset{Table\,2}{\approx} \frac{1}{2}\alpha\int_0^L \begin{bmatrix}V^*\\ \Omega^*\\ \gamma^*\\ \kappa^*\end{bmatrix}^T \begin{bmatrix}\mathbb{G} & \mathbb{K} & 0 & 0\\ \mathbb{K}^T & \mathbb{I} & 0 & 0\\ 0 & 0 & \mathbb{U} & \mathbb{V}\\ 0 & 0 & \mathbb{V}^T & \mathbb{W}\end{bmatrix} \begin{bmatrix}V^*\\ \Omega^*\\ \gamma^*\\ \kappa^*\end{bmatrix} dx \overset{Table\,1}{=} \alpha\left(T^* + V^*\right), \tag{28}$$

where $()^*$ denotes variables measured from the steady state, e.g. $V^* \approx \Phi^V\mathbf{Tq}$, whereas $V \approx \Phi^V(\mathbf{Tq}+q^0)$. Consequently, T^* and U^* denote a pseudo kinetic and potential energy of the blade. If the steady state solution is zero ($q^0 = 0$), $T^* = T$ and $U^* = U$ are the physical kinetic and potential energy. Eq. (26) can be written with Eq. (28) as

$$J = E\left\{\lim_{T\to\infty}\frac{1}{T}\int_0^T \left[\alpha\left(T^* + U^*\right) + u^T u\right]dt\right\} \to min. \tag{29}$$

The compromise between the blade energy minimization and the minimization of the control effort can be adjusted by a single parameter α.

For the Kalman filter design of the LQG controller, it is assumed that the process and measurement noise is white and Gaussian. The covariance of the external force f^{dist}, and the external moment m^{dist}, as well as the covariance of the measurement noise w, which affects the measurement as $y_y = \mathbf{M}_{yr}\mathbf{q}_r + w + y_y^0$, are chosen as

$$E\{f^{dist}f^{dist^T}\} = \begin{bmatrix} 1 & 0 & 0 \\ 0 & 1 & 0 \\ 0 & 0 & 10 \end{bmatrix}, \quad E\{m^{dist}m^{dist^T}\} = \begin{bmatrix} 0.01 & 0 & 0 \\ 0 & 0.01 & 0 \\ 0 & 0 & 0.01 \end{bmatrix}, \quad E\{ww^T\} = 10^{-5}\, I. \tag{30}$$

The process noise is chosen such that f_3 dominates, which is the force required for the lift of the blade, while the process noise is equal for each element of w since all measurements are performed by the same type of sensors.

Closed-Loop Results

The control design is performed based on a reduced model using the first 6 normal modes (12^{th} order model). The controller is tested on a model with 12 normal modes (24^{th} order model). For the control design we chose the covariance matrices as presented in (30), α is chosen as 10^8, and the other parameters are as specified in Table 4. The exact values of the natural frequencies and damping for the controlled and uncontrolled blade are presented in Table 7. Note that the frequency of the 1^{st} torsion mode changes more than other modes because of the large aerodynamic loads induced by the 1^{st} torsion mode.

In order to validate the controller, a simulation is conducted starting at the steady state, where the controller is switched off for 0.5 seconds, followed by a linear increase in the control gain so that it is fully active at $t = 0.6$ seconds. As can be seen in Fig. 7, there is a considerable decrease of the blade energy when the controller is switched on.

Figure 8 shows the effect of the controller on the generalized velocities and strains relative to the steady state. The generalized strains at the root are plotted as these are typically the maximum values. The same holds for the generalized velocities at the tip. The maximum measured voltage was 200 V which is considerably less than the voltage saturation of 1000 V (see [Ref. 2]).

Conclusions

The paper shows an effective way to analyze, simulate and control active helicopter blades. It takes advantage of the Galerkin approach to efficiently represent the nonlinear blade dynamics in a quadratic form. The analysis showed the importance of the aerodynamics on the blade model as it adds significant damping. A nonlinear order reduction method has been presented which can be useful for control design as well as computationally efficient time marching simulations. It exploits the potential of normal modes in capturing the nonlinear blade dynamics. Finally, an energy optimal LQG control design has been performed that provides additional damping for the helicopter blade.

Appendix

The tensors of the discretized blade model are given for the special case of a constant cross-section (varying cross-sections are also possible). To ensure a proper formulation of the tensor calculations, a hierarchical tensor notation is introduced.

Hierarchical tensor notation

Consider the approximation $V = \Phi_i^V q_i$ where each Φ_i^V is a 3×12 matrix and each q_i is a 12×1 vector. Now, define $\Phi_{i(a)}$ and $q_{i(a)}$ with $a = 1...12$ where $V = \Phi_{i(a)}^V q_{i(a)}$ is summarized in an inner loop over a and in an outer loop over i. Consequently, $\Phi_{i(a)}^V$ becomes a 3×1 vector and $q_{i(a)}$ a scalar. This definition is necessary to e.g. obtain the $\mathcal{C}^{struc}$-tensor where the tilde operator is used which is defined for 3×1 vectors only. Note that for simplicity, the hierarchical structure is often suppressed.

Abbreviations

In order to obtain a compact formulation of the tensor calculation, some abbreviations are introduced. First, the Ψ constants are introduced:

$$\Psi^V = \left[I\ 0\ 0\ 0 \right], \qquad \Psi^\Omega = \left[0\ I\ 0\ 0 \right], \qquad \Psi^\gamma = \left[0\ 0\ I\ 0 \right], \qquad \Psi^\kappa = \left[0\ 0\ 0\ I \right], \tag{31}$$

where I is a 3×3 identity matrix. The abbreviations used for the Legendre functions are:

$$S_k^{\mathbb{0}} = P_k(\mathbb{0}), \qquad S_k^{\mathbb{L}} = P_k(\mathbb{L}), \qquad D_{ki}^{\mathbb{0}} = P_k(\mathbb{0})P_i(\mathbb{0}), \qquad D_{ki}^{\mathbb{L}} = P_k(\mathbb{L})P_i(\mathbb{L}), \qquad S_{ku}^{\mathbb{L}seg} = \begin{cases} P_k(\mathbb{L}), & u = 6 \\ 0, & u \neq 6 \end{cases} \tag{32}$$

The abbreviations of the Legendre integrals are:

$$\begin{aligned} S_k^{\int} &= \mathbb{L}\int_{\mathbb{0}}^{1}\Big\{P_k(\bar{x})\Big\}d\bar{x}, & S_{ku}^{\int seg} &= \mathbb{L}\int_{(u-1)\frac{\mathbb{1}}{6}}^{u\frac{\mathbb{1}}{6}}\Big\{P_k(\bar{x})\Big\}d\bar{x}, \\ D_{ki}^{\int} &= \mathbb{L}\int_{\mathbb{0}}^{1}\Big\{P_k(\bar{x})P_i(\bar{x})\Big\}d\bar{x}, & {}^{d}S_{ku}^{\int seg} &= \int_{(u-1)\frac{\mathbb{1}}{6}}^{u\frac{\mathbb{1}}{6}}\Big\{P_k'(\bar{x})\Big\}d\bar{x}, \\ {}^{d}D_{ki}^{\int} &= \int_{\mathbb{0}}^{1}\Big\{P_k(\bar{x})P_i'(\bar{x})\Big\}d\bar{x}, & D_{kiu}^{\int seg} &= \mathbb{L}\int_{(u-1)\frac{\mathbb{1}}{6}}^{u\frac{\mathbb{1}}{6}}\Big\{P_k(\bar{x})P_i(\bar{x})\Big\}d\bar{x}, \\ T_{kij}^{\int} &= \mathbb{L}\int_{\mathbb{0}}^{1}\Big\{P_k(\bar{x})P_i(\bar{x})P_j(\bar{x})\Big\}d\bar{x}. \end{aligned} \tag{33}$$

Tensor calculations

$$\begin{aligned} \mathcal{A}_{k(c)i(a)} = D_{ki}^{\int} \Big\{ & {\Psi_{(c)}^{V}}^{T}\Big[\mathbb{G}\Psi_{(a)}^{V} + \mathbb{K}\Psi_{(a)}^{\Omega}\Big] + {\Psi_{(c)}^{\Omega}}^{T}\Big[\mathbb{K}^{T}\Psi_{(a)}^{V} + \mathbb{I}\Psi_{(a)}^{\Omega}\Big] \\ & + (\mathbb{U}\Psi_{(c)}^{\gamma} + \mathbb{V}\Psi_{(c)}^{\kappa})^{T}\Big[\Psi_{(a)}^{\gamma}\Big] + (\mathbb{V}^{T}\Psi_{(c)}^{\gamma} + \mathbb{W}\Psi_{(c)}^{\kappa})^{T}\Big[\Psi_{(a)}^{\kappa}\Big]\Big\}, \end{aligned}$$

$$\begin{aligned} \mathcal{B}_{k(c)i(a)}^{no\,BC} = {}^{d}D_{ki}^{\int} \Big\{ & {\Psi_{(c)}^{V}}^{T}\Big[-\mathbb{U}\Psi_{(a)}^{\gamma} - \mathbb{V}\Psi_{(a)}^{\kappa}\Big] + {\Psi_{(c)}^{\Omega}}^{T}\Big[-\mathbb{V}^{T}\Psi_{(a)}^{\gamma} - \mathbb{W}\Psi_{(a)}^{\kappa}\Big] \\ & + (\mathbb{U}\Psi_{(c)}^{\gamma} + \mathbb{V}\Psi_{(c)}^{\kappa})^{T}\Big[-\Psi_{(a)}^{V}\Big] + (\mathbb{V}^{T}\Psi_{(c)}^{\gamma} + \mathbb{W}\Psi_{(c)}^{\kappa})^{T}\Big[-\Psi_{(a)}^{\Omega}\Big]\Big\} \\ + D_{ki}^{\int} \Big\{ & -{\Psi_{(c)}^{V}}^{T}\Big[\tilde{\mathbb{k}}(\mathbb{U}\Psi_{(a)}^{\gamma} + \mathbb{V}\Psi_{(a)}^{\kappa})\Big] - {\Psi_{(c)}^{\Omega}}^{T}\Big[\tilde{\mathbb{k}}(\mathbb{V}^{T}\Psi_{(a)}^{\gamma} + \mathbb{W}\Psi_{(a)}^{\kappa}) - \tilde{e}_1(\mathbb{U}\Psi_{(a)}^{\gamma} + \mathbb{V}\Psi_{(a)}^{\kappa})\Big] \\ & - (\mathbb{U}\Psi_{(c)}^{\gamma} + \mathbb{V}\Psi_{(c)}^{\kappa})^{T}\Big[\tilde{\mathbb{k}}\Psi_{(a)}^{V} - \tilde{e}_1\Psi_{(a)}^{\Omega}\Big] - (\mathbb{V}^{T}\Psi_{(c)}^{\gamma} + \mathbb{W}\Psi_{(c)}^{\kappa})^{T}\Big[\tilde{\mathbb{k}}\Psi_{(a)}^{\Omega}\Big]\Big\}, \end{aligned} \tag{34}$$

$$\begin{aligned} \mathcal{C}_{k(c)i(a)j(b)}^{struc} = T_{kij}^{\int} \Big\{ & {\Psi_{(c)}^{V}}^{T}\Big[-\tilde{\Psi}_{(a)}^{\kappa}(\mathbb{U}\Psi_{(b)}^{\gamma} + \mathbb{V}\Psi_{(b)}^{\kappa}) + \tilde{\Psi}_{(a)}^{\Omega}(\mathbb{G}\Psi_{(b)}^{V} + \mathbb{K}\Psi_{(b)}^{\Omega})\Big] \\ & + {\Psi_{(c)}^{\Omega}}^{T}\Big[\tilde{\Psi}_{(a)}^{\Omega}(\mathbb{K}^{T}\Psi_{(b)}^{V} + \mathbb{I}\Psi_{(b)}^{\Omega}) + \tilde{\Psi}_{(a)}^{V}(\mathbb{G}\Psi_{(b)}^{V} + \mathbb{K}\Psi_{(b)}^{\Omega}) - \tilde{\Psi}_{(a)}^{\kappa}(\mathbb{V}^{T}\Psi_{(b)}^{\gamma} \\ & \quad + \mathbb{W}\Psi_{(b)}^{\kappa}) - \tilde{\Psi}_{(a)}^{\gamma}(\mathbb{U}\Psi_{(b)}^{\gamma} + \mathbb{V}\Psi_{(b)}^{\kappa})\Big] \\ & + (\mathbb{U}\Psi_{(c)}^{\gamma} + \mathbb{V}\Psi_{(c)}^{\kappa})^{T}\Big[-\tilde{\Psi}_{(a)}^{\kappa}\Psi_{(b)}^{V} - \tilde{\Psi}_{(a)}^{\gamma}\Psi_{(b)}^{\Omega}\Big] + (\mathbb{V}^{T}\Psi_{(c)}^{\gamma} + \mathbb{W}\Psi_{(c)}^{\kappa})^{T}\Big[-\tilde{\Psi}_{(a)}^{\kappa}\Psi_{(b)}^{\Omega}\Big]\Big\}. \end{aligned}$$

The tensor calculating the aerodynamic force and moment is:

$$\begin{aligned} \mathcal{C}_{k(c)i(a)j(b)}^{aero} = T_{kij}^{\int} \Big\{ & {\Psi_{(c)}^{V}}^{T}\Big\{0\ 1\ 0\Big\}^{T}\Big[{\Psi_{(a)}^{V}}^{T}\mathbb{X}^{VV}\Psi_{(b)}^{V} + {\Psi_{(a)}^{V}}^{T}\mathbb{X}^{V\Omega}\Psi_{(b)}^{\Omega} + {\Psi_{(a)}^{\Omega}}^{T}\mathbb{X}^{\Omega\Omega}\Psi_{(b)}^{\Omega}\Big] \\ & + {\Psi_{(c)}^{V}}^{T}\Big\{0\ 0\ 1\Big\}^{T}\Big[{\Psi_{(a)}^{V}}^{T}\mathbb{Y}^{VV}\Psi_{(b)}^{V} + {\Psi_{(a)}^{V}}^{T}\mathbb{Y}^{V\Omega}\Psi_{(b)}^{\Omega}\Big] \\ & + {\Psi_{(c)}^{\Omega}}^{T}\Big\{1\ 0\ 0\Big\}^{T}\Big[{\Psi_{(a)}^{V}}^{T}\mathbb{Z}^{VV}\Psi_{(b)}^{V} + {\Psi_{(a)}^{V}}^{T}\mathbb{Z}^{V\Omega}\Psi_{(b)}^{\Omega}\Big]\Big\}. \end{aligned} \tag{35}$$

The actuation for constant cross-section is determined by:

$$\begin{aligned}\mathcal{E}^{no\,BC}_{k(c)u} &= {}^{d}S^{\int seg}_{ku}\left\{ {\Psi^{V}_{(c)}}^{T}(\mathbb{U}\mathbb{E}+\mathbb{V}\mathbb{F})+{\Psi^{\Omega}_{(c)}}^{T}(\mathbb{V}^{T}\mathbb{E}+\mathbb{W}\mathbb{F})\right\}\\ &+S^{\int seg}_{ku}\left\{ {\Psi^{V}_{(c)}}^{T}\left[\tilde{\mathbb{k}}\right](\mathbb{U}\mathbb{E}+\mathbb{V}\mathbb{F})+{\Psi^{\Omega}_{(c)}}^{T}\left[\tilde{\mathbb{k}}\right](\mathbb{V}^{T}\mathbb{E}+\mathbb{W}\mathbb{F})+{\Psi^{\Omega}_{(c)}}^{T}\left[\tilde{e}_{1}\right](\mathbb{U}\mathbb{E}+\mathbb{V}\mathbb{F})\right\},\end{aligned} \tag{36}$$

$$\mathcal{F}^{no\,BC}_{k(c)i(a)u} = D^{\int seg}_{kiu}\left\{ {\Psi^{V}_{(c)}}^{T}\left[\tilde{\Psi}^{\kappa}_{(a)}\right](\mathbb{U}\mathbb{E}+\mathbb{V}\mathbb{F})+{\Psi^{\Omega}_{(c)}}^{T}\left[\tilde{\Psi}^{\kappa}_{(a)}\right](\mathbb{V}^{T}\mathbb{E}+\mathbb{W}\mathbb{F})+{\Psi^{\Omega}_{(c)}}^{T}\left[\tilde{\Psi}^{\gamma}_{(a)}\right](\mathbb{U}\mathbb{E}+\mathbb{V}\mathbb{F})\right\}.$$

f_k and m_k are:

$$\begin{aligned}f_{k(c)} &= S^{\int}_{k}\left\{ -{\Psi^{V}_{(c)}}^{T}f\right\},\\ m_{k(c)} &= S^{\int}_{k}\left\{ -{\Psi^{\Omega}_{(c)}}^{T}m\right\}.\end{aligned} \tag{37}$$

The tensors occurring due to boundary conditions are:

$$\begin{aligned}\mathcal{D}^{BC}_{k(c)} &= S^{\mathbb{0}}_{k}\left\{ \left(\mathbb{U}\Psi^{\gamma}_{(c)}+\mathbb{V}\Psi^{\kappa}_{(c)}\right)^{T}V^{\mathbb{0}}+\left(\mathbb{V}^{T}\Psi^{\gamma}_{(c)}+\mathbb{W}\Psi^{\kappa}_{(c)}\right)^{T}\Omega^{\mathbb{0}}\right\}\\ &+S^{\mathbb{L}}_{k}\left\{ -{\Psi^{V}_{(c)}}^{T}F^{\mathbb{L}}-{\Psi^{\Omega}_{(c)}}^{T}M^{\mathbb{L}}\right\},\end{aligned}$$

$$\begin{aligned}\mathcal{B}^{BC}_{k(c)i(a)} &= D^{\mathbb{0}}_{ki}\left\{ -\left(\mathbb{U}\Psi^{\gamma}_{(c)}+\mathbb{V}\Psi^{\kappa}_{(c)}\right)^{T}\left[\Psi^{V}_{(a)}\right]-\left(\mathbb{V}^{T}\Psi^{\gamma}_{(c)}+\mathbb{W}\Psi^{\kappa}_{(c)}\right)^{T}\left[\Psi^{\Omega}_{(a)}\right]\right\}\\ &+D^{\mathbb{L}}_{ki}\left\{ {\Psi^{V}_{(c)}}^{T}\left[\mathbb{U}\Psi^{\gamma}_{(a)}+\mathbb{V}\Psi^{\kappa}_{(a)}\right]+{\Psi^{\Omega}_{(c)}}^{T}\left[\mathbb{V}^{T}\Psi^{\gamma}_{(a)}+\mathbb{W}\Psi^{\kappa}_{(a)}\right]\right\},\end{aligned} \tag{38}$$

$$\mathcal{E}^{BC}_{k(c)u} = S^{\mathbb{L}seg}_{ku}\left\{ -{\Psi^{V}_{(c)}}^{T}(\mathbb{U}\mathbb{E}+\mathbb{V}\mathbb{F})-{\Psi^{\Omega}_{(c)}}^{T}(\mathbb{V}^{T}\mathbb{E}+\mathbb{W}\mathbb{F})\right\}.$$

The measurement tensors is:

$$\mathcal{M}_{yi(a)} = \left\{\begin{matrix}\Psi^{\gamma}\\ \Psi^{\kappa}\end{matrix}\right\}P_{i(a)}\left(\frac{y-1}{4}\right). \tag{39}$$

References

[1]Shin, S. J. and Cesnik, C. E. S., "Helicopter performance and vibration enhancement by twist-actuated blades," Paper AIAA 2003-1818, 44th AIAA/ASME/ASCE/AHS Structures, Structural Dynamics, and Materials Conference Proceedings, Norfolk, VA, April 7-10 2003.

[2]Wilbur, M. L., Mirick, P. H., Yeager, W. T., Langston, C. W., Cesnik C. E. S., and Shin, S., "Vibratory loads reduction testing of the NASA/Army/MIT active twist rotor," *Journal of the American Helicopter Society*, Vol. 47, (2), April 2002, pp. 123 – 133.

[3]Traugott, J. P., Patil, M. J., and Holzapfel, F., "Nonlinear dynamics and control of integrally actuated helicopter blades," Paper AIAA-2005-2271, 13th AIAA/ASME/AHS Adaptive Structures Conference Proceedings, Austin, TX, April 18 - 21 2005.

[4]Patil, M. J., and Althoff, M., "Energy-consistent, Galerkin approach for the nonlinear dynamics of beams using mixed, intrinsic equations," Paper AIAA 2006-1737, 47th AIAA/ASME/ASCE/AHS/ASC Structures, Structural Dynamics and Materials Conference Proceedings, Newport, RI, May 1-4 2006.

[5]Patil, M. J., and Hodges, D. H., "Flight dynamics of highly flexible flying wings," International Forum on Aeroelasticity and Structural Dynamics Proceedings, Munich, Germany, 28 June - 01 July 2005.

[6]Hodges, D. H., "A mixed variational formulation based on exact intrinsic equations for dynamics of moving beams," *International Journal of Solids and Structures*, Vol. 26, (11), 1990, pp. 1253 – 1273.

[7]Hodges, D. H., "Geometrically exact, intrinsic theory for dynamics of curved and twisted anisotropic beams," *AIAA Journal*, Vol. 41, (6), 2003, pp.1131– 1137.

[8]Hopkins, A. S., and Ormiston, R. A., "An examination of selected problems in rotor blade structural mechanics and dynamics," American Helicopter Society 59th Annual Forum Proceedings, Phoenix, AZ, May 6-8 2003.

[9]Patil, M. J., and Johnson, E. R., "Cross-sectional analysis of anisotropic, thin-walled, closed-section beams with embedded strain actuation," Paper AIAA-2005-2037, 13th AIAA/ASME/AHS Adaptive Structures Conference Proceedings, Austin, TX, April 18 - 21 2005.

[10]Cesnik C. E. S., and Palacios, R., "Modeling piezocomposite actuators embedded in slender struc-

tures," Paper AIAA 2003-1803, 44th AIAA/ASME/ASCE/AHS Structures, Structural Dynamics, and Materials Conference Proceedings, Norfolk, VA, April 7-10 2003.

[11]Peters, D. A., and Johnson, M. J., "Finite-state airloads for deformable airfoils on fixed and rotating wings," Symposium on Aeroelasticity and Fluid/Structure Interaction, Proceedings of the Winter Annual Meeting, Chicago, IL, November 6-11 1994.

[12]Fletcher, C. A. J., *Computational Galerkin Methods*. Springer, New York, NY, 1984.

[13]Abramowitz, M., and Stegun, A., *Handbook of Mathematical Functions*. Dover, New York, NY, 1964.

[14]Patil, M. J., "Decoupled second-order equations and modal analysis of a general non-conservative system," Paper AIAA-2000-1654, AIAA Dynamics Specialists Conference Proceedings, Atlanta, GA, April 5-6 2000.

[15]Noor, A. K., and Peters, J. M., "Reduced basis technique for nonlinear analysis of structures," *AIAA Journal*, Vol. 18, (4), April 1980, pp. 455–462.

[16]Bauchau, O. A., and Guernsey, D., "On the choice of appropriate bases for nonlinear dynamic modal analysis," *Journal of the American Helicopter Society*, Vol. 38, (4), October 1993, pp. 28–36.

[17]Burl, J. B., *Linear Optimal Control*. Addison-Wesley Longman Publishing, Boston, MA, November 1998.

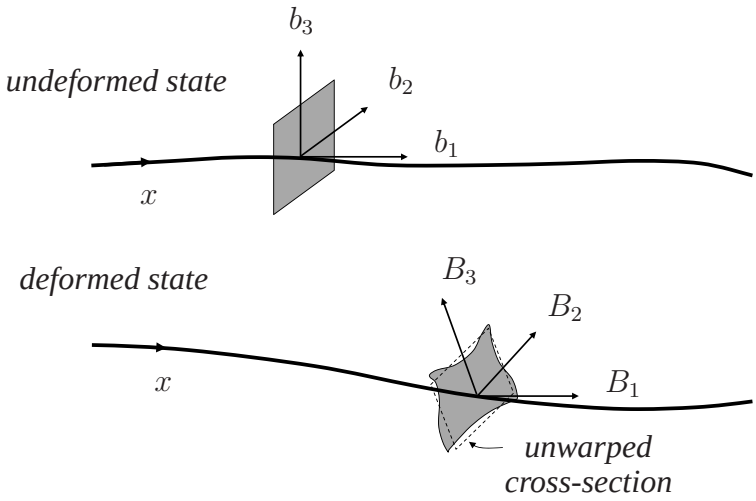

Fig. 1 Schematic of a beam undergoing finite deformation and cross-sectional warping.

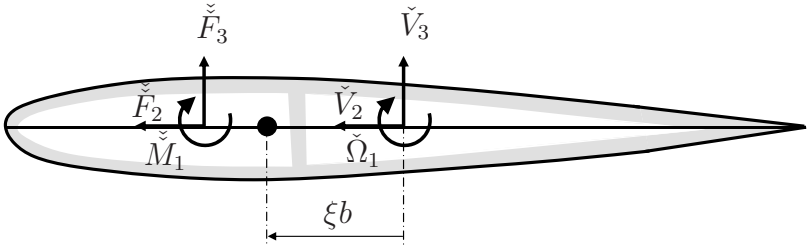

Fig. 2 Velocities and aerodynamic forces within the blade profile.

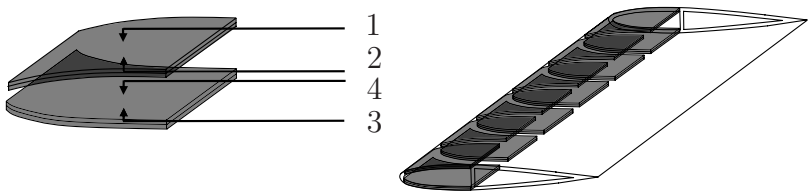

Fig. 3 Actuator distribution in an integrally actuated blade.

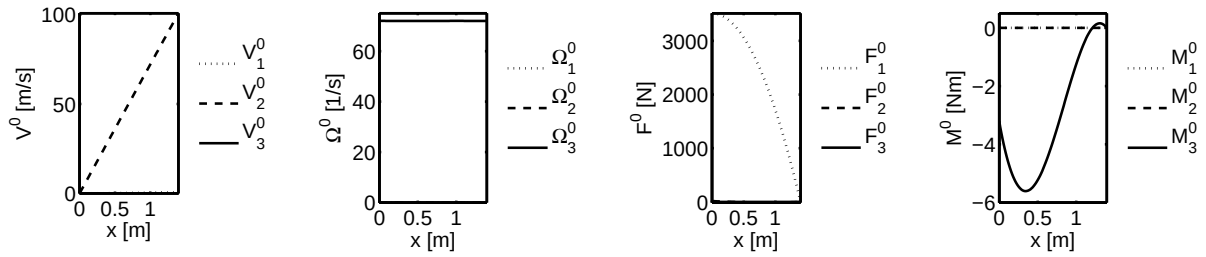

(a) Steady State of V (b) Steady State of Ω (c) Steady State of F (d) Steady State of M

Fig. 4 Steady state solution for V, Ω, F and M.

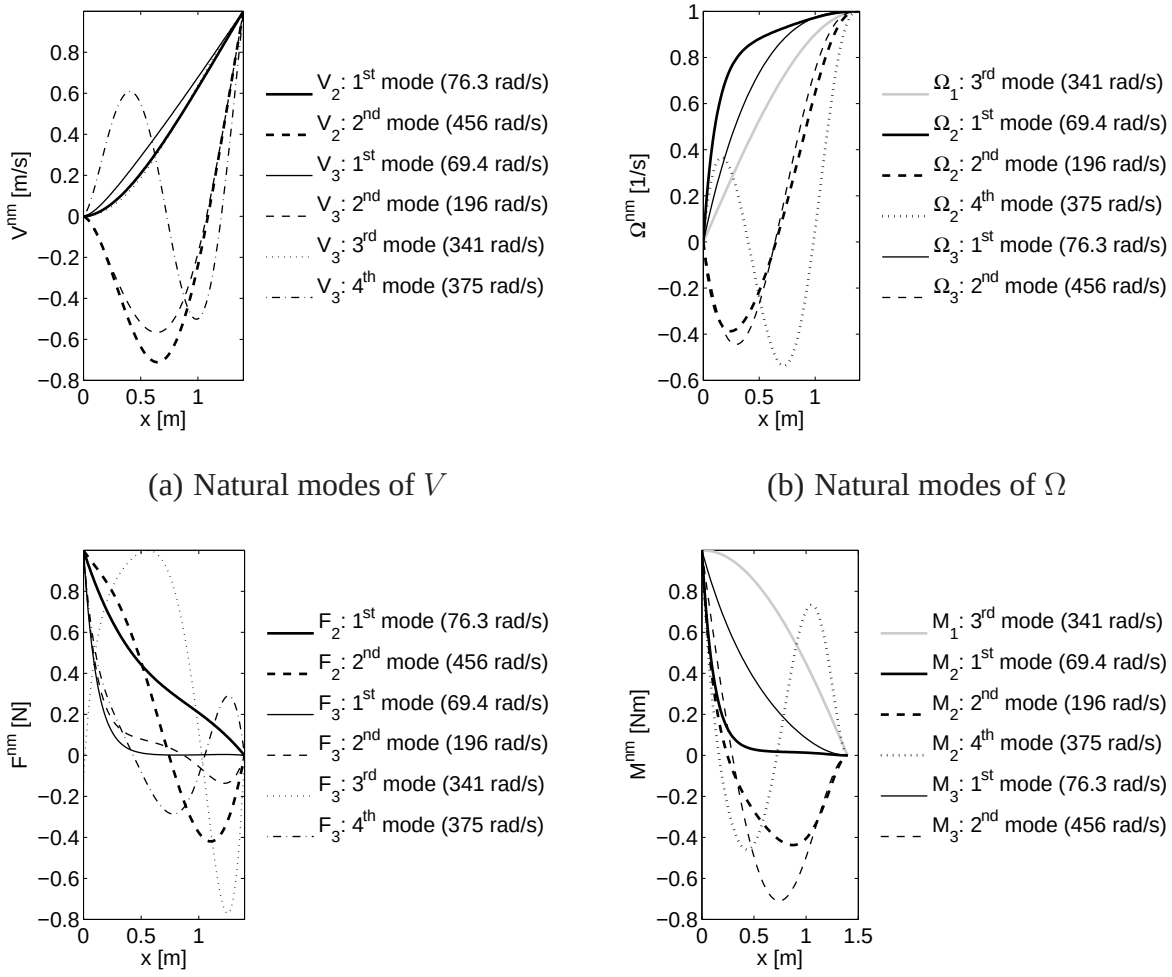

(a) Natural modes of V

(b) Natural modes of Ω

(c) Natural modes of F

(d) Natural modes of M

Fig. 5 Natural modes of helicopter blade.

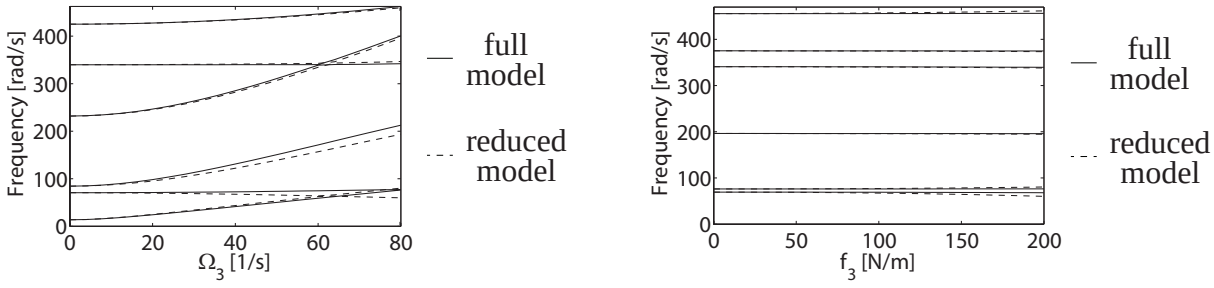

(a) Frequencies under varying rotational speed Ω_3.

(b) Frequencies under varying external force f_3.

Fig. 6 Frequencies of the full and reduced model.

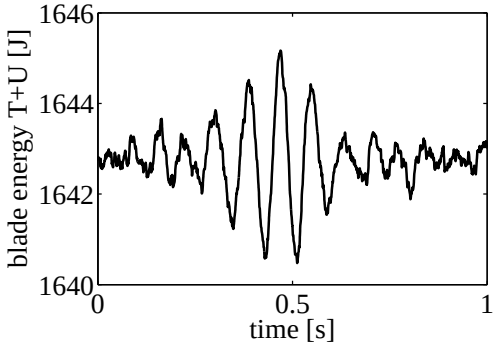

Fig. 7 Blade energy $T + U$.

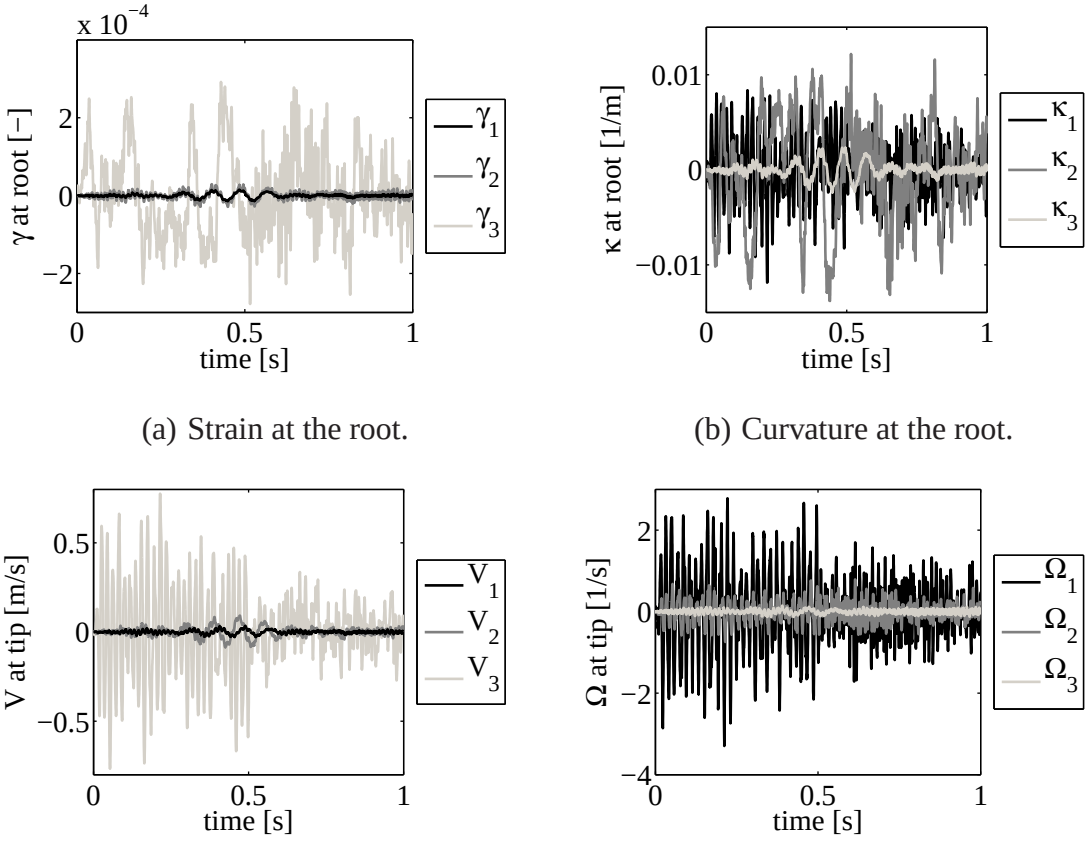

(a) Strain at the root.

(b) Curvature at the root.

(c) Linear velocity at the tip.

(d) Angular velocity at the tip.

Fig. 8 Simulation results for $\gamma(\mathbb{0})$, $\kappa(\mathbb{0})$, $V(\mathbb{L})$ and $\Omega(\mathbb{L})$.

Table 1. Energies in the active helicopter blade.

Change of kinetic energy	$\dot{T}$	$= \int_0^L \left[V^T \dot{P} + \Omega^T \dot{H} \right] dx$
Change of potential energy	$\dot{U}$	$= \int_0^L \left[(F + F^A)^T \dot{\gamma} + (M + M^A)^T \dot{\kappa} \right] dx$
External power	P^{ext}	$= \int_0^L \left[V^T f + \Omega^T m \right] dx$
Boundary power	P^{bou}	$= V(\mathbb{L})^T F^{\mathbb{L}} + \Omega(\mathbb{L})^T M^{\mathbb{L}} - F(\mathbb{0})^T V^{\mathbb{0}} - M(\mathbb{0})^T \Omega^{\mathbb{0}}$
Estimated actuation power	P^{act*}	$\approx \int_0^L \left[{F^A}^T \dot{\gamma} + {M^A}^T \dot{\kappa} \right] dx$

Table 2. Assumed spatial modes and time functions of the approximated variables.

$V(x,t)$	=	$\bar{V}_l(x)v_l(t)$	=	$\Phi_l^V(x)q_l(t)$	$\Phi_l^V(x)$	=	$\left[\right.$	$\bar{V}_l$	0	0	0 $\left.\right]$
$\Omega(x,t)$	=	$\bar{\Omega}_l(x)\omega_l(t)$	=	$\Phi_l^\Omega(x)q_l(t)$	$\Phi_l^\Omega(x)$	=	$\left[\right.$	0	$\bar{\Omega}_l$	0	0 $\left.\right]$
$\gamma(x,t)$	=	$\bar{\gamma}_l(x)g_l(t)$	=	$\Phi_l^\gamma(x)q_l(t)$	$\Phi_l^\gamma(x)$	=	$\left[\right.$	0	0	$\bar{\gamma}_l$	0 $\left.\right]$
$\kappa(x,t)$	=	$\bar{\kappa}_l(x)k_l(t)$	=	$\Phi_l^\kappa(x)q_l(t)$	$\Phi_l^\kappa(x)$	=	$\left[\right.$	0	0	0	$\bar{\kappa}_l$ $\left.\right]$
[3 × 1]		[3 × 3][3 × 1]		[3 × 12][12 × 1]	$q_l(t)$	=	$\left\{\right.$	$v_l(t)$	$\omega_l(t)$	$g_l(t)$	$k_l(t)$ $\left.\right\}^T$

Table 3. Free vibration solution (fvs) and natural modes (nm).

$V_l^{fvs}(x,t)$	=	$c_l V_l^{nm}(x) \left\{ e^{\lambda_l t}\ e^{\hat{\lambda}_l t} \right\}^T$	$V_l^{nm}(x)$	=	$\Phi_i^V(x)\mathbf{T}_{il}$
$\Omega_l^{fvs}(x,t)$	=	$c_l \Omega_l^{nm}(x) \left\{ e^{\lambda_l t}\ e^{\hat{\lambda}_l t} \right\}^T$	$\Omega_l^{nm}(x)$	=	$\Phi_i^\Omega(x)\mathbf{T}_{il}$
$\gamma_l^{fvs}(x,t)$	=	$c_l \gamma_l^{nm}(x) \left\{ e^{\lambda_l t}\ e^{\hat{\lambda}_l t} \right\}^T$	$\gamma_l^{nm}(x)$	=	$\Phi_i^\gamma(x)\mathbf{T}_{il}$
$\kappa_l^{fvs}(x,t)$	=	$c_l \kappa_l^{nm}(x) \left\{ e^{\lambda_l t}\ e^{\hat{\lambda}_l t} \right\}^T$	$\kappa_l^{nm}(x)$	=	$\Phi_i^\kappa(x)\mathbf{T}_{il}$
$[3 \times 1]$		$[1 \times 1][3 \times 2][2 \times 1]$	$[3 \times 2]$		$[3 \times 12][12 \times 2]$

Table 4. Parameters of the helicopter blade.

Structure Parameters			
$\mathbb{R} = \begin{bmatrix} \mathbb{R}_{11} & 0 & 0 \\ 0 & \mathbb{R}_{22} & 0 \\ 0 & 0 & \mathbb{R}_{33} \end{bmatrix}$,	$\mathbb{S} = \begin{bmatrix} 0 & 0 & \mathbb{S}_{13} \\ 0 & 0 & 0 \\ \mathbb{S}_{31} & 0 & 0 \end{bmatrix}$,	$\mathbb{T} = \begin{bmatrix} \mathbb{T}_{11} & 0 & 0 \\ 0 & \mathbb{T}_{22} & 0 \\ 0 & 0 & \mathbb{T}_{33} \end{bmatrix}$	
$\mathbb{R}_{11} = 6.4375 \cdot 10^{-7}$,	$\mathbb{R}_{22} = 4.9262 \cdot 10^{-6}$,	$\mathbb{R}_{33} = 4.4389 \cdot 10^{-5}$,	$\mathbb{S}_{13} = 5.5420 \cdot 10^{-6}$
$\mathbb{S}_{31} = 1.8621 \cdot 10^{-4}$,	$\mathbb{T}_{11} = 2.9086 \cdot 10^{-2}$,	$\mathbb{T}_{22} = 2.5038 \cdot 10^{-2}$,	$\mathbb{T}_{33} = 9.2640 \cdot 10^{-4}$
$\mu = 6.9310 \cdot 10^{-1}$,	$\xi_2 = -6.9240 \cdot 10^{-4}$,	$\xi_3 = 0$,	$\mathbb{i}_2 = 6.4630 \cdot 10^{-6}$
$\mathbb{i}_3 = 3.7018 \cdot 10^{-4}$,	$\mathbb{i}_{23} = 0$,	$\mathbb{L} = 1.3970$	
Actuation Parameters			
$\mathbb{E} = \begin{bmatrix} \mathbb{E}_{11} & 0 & 0 \\ 0 & \mathbb{E}_{22} & 0 \\ 0 & 0 & \mathbb{E}_{33} \end{bmatrix} \begin{bmatrix} +1 & +1 & +1 & +1 \\ +1 & -1 & -1 & +1 \\ +1 & -1 & +1 & -1 \end{bmatrix}$,		$\mathbb{F} = \begin{bmatrix} \mathbb{F}_{11} & 0 & 0 \\ 0 & \mathbb{F}_{22} & 0 \\ 0 & 0 & \mathbb{F}_{33} \end{bmatrix} \begin{bmatrix} -1 & +1 & -1 & +1 \\ +1 & +1 & -1 & -1 \\ +1 & +1 & +1 & +1 \end{bmatrix}$	
$\mathbb{E}_{11} = 8.9562 \cdot 10^{-9}$,	$\mathbb{E}_{22} = 2.7843 \cdot 10^{-8}$,	$\mathbb{E}_{33} = 2.8536 \cdot 10^{-8}$,	
$\mathbb{F}_{11} = 3.8506 \cdot 10^{-6}$	$\mathbb{F}_{22} = 1.9155 \cdot 10^{-6}$,	$\mathbb{F}_{33} = 8.5769 \cdot 10^{-8}$	
Aerodynamic Parameters			
$\rho = 1.2$,	$b = 5.3850 \cdot 10^{-2}$,	$\xi = 0.5$,	$C_{l\alpha} = 2\pi$
$C_{l0} = 0$,	$C_{d0} = 0.01$,	$C_{m0} = 0$	

Table 5. Natural frequencies of aeroelastic and structural models.

Mode		Aeroelastic Model		NATASHA: Aeroelastic Model		Structural Model	
		frequency (rad/s)	damping ratio (—)	frequency (rad/s)	damping ratio (—)	frequency (rad/s)	damping ratio (—)
1^{st}	bending	69.4195	$+3.26373 \cdot 10^{-1}$	69.4197	$+3.26346 \cdot 10^{-1}$	75.9873	$+3.08857 \cdot 10^{-13}$
2^{nd}	bending	196.286	$+9.35641 \cdot 10^{-2}$	196.410	$+9.34763 \cdot 10^{-2}$	199.654	$-2.17091 \cdot 10^{-14}$
3^{rd}	bending	375.224	$+4.30848 \cdot 10^{-2}$	376.198	$+4.29394 \cdot 10^{-2}$	376.570	$-1.20760 \cdot 10^{-15}$
4^{th}	bending	609.286	$+2.47827 \cdot 10^{-2}$	612.750	$+2.46039 \cdot 10^{-2}$	610.149	$+2.74831 \cdot 10^{-15}$
5^{th}	bending	890.557	$+1.62854 \cdot 10^{-2}$	899.274	$+1.60790 \cdot 10^{-2}$	891.379	$+4.23075 \cdot 10^{-15}$
6^{th}	bending	1212.55	$+1.16096 \cdot 10^{-2}$	1230.60	$+1.14019 \cdot 10^{-2}$	1213.28	$-7.26892 \cdot 10^{-14}$
1^{st}	lead-lag	76.2633	$+9.82787 \cdot 10^{-4}$	76.2685	$+9.81159 \cdot 10^{-4}$	76.2633	$+1.26594 \cdot 10^{-14}$
2^{nd}	lead-lag	455.697	$+1.20758 \cdot 10^{-4}$	456.288	$+1.21496 \cdot 10^{-4}$	455.700	$+1.19983 \cdot 10^{-14}$
3^{rd}	lead-lag	1158.70	$+4.12947 \cdot 10^{-5}$	1162.77	$+4.41446 \cdot 10^{-5}$	1158.69	$+1.50088 \cdot 10^{-15}$
1^{st}	torsion	340.945	$+7.47685 \cdot 10^{-2}$	340.972	$+7.47336 \cdot 10^{-2}$	346.387	$-6.40185 \cdot 10^{-14}$
2^{nd}	torsion	1019.34	$+1.90722 \cdot 10^{-2}$	1020.14	$+1.90621 \cdot 10^{-2}$	1021.03	$-5.40023 \cdot 10^{-15}$

Table 6. Assumed modes and time functions for the reduced order model.

$V(x,t)$	=	$V^0(x) + \mathbf{\Phi}_r^V(x)\mathbf{q}_r(t)$		$V^0(x)$	=	$\Phi_l^V(x)q_l^0$	,	$\mathbf{\Phi}_r^V(x)$	=	$\Phi_l^V(x)\mathbf{T}_{lr}$	
$\Omega(x,t)$	=	$\Omega^0(x) + \mathbf{\Phi}_r^\Omega(x)\mathbf{q}_r(t)$		$\Omega^0(x)$	=	$\Phi_l^\Omega(x)q_l^0$	,	$\mathbf{\Phi}_r^\Omega(x)$	=	$\Phi_l^\Omega(x)\mathbf{T}_{lr}$	
$\gamma(x,t)$	=	$\gamma^0(x) + \mathbf{\Phi}_r^\gamma(x)\mathbf{q}_r(t)$		$\gamma^0(x)$	=	$\Phi_l^\gamma(x)q_l^0$	,	$\mathbf{\Phi}_r^\gamma(x)$	=	$\Phi_l^\gamma(x)\mathbf{T}_{lr}$	
$\kappa(x,t)$	=	$\kappa^0(x) + \mathbf{\Phi}_r^\kappa(x)\mathbf{q}_r(t)$		$\kappa^0(x)$	=	$\Phi_l^\kappa(x)q_l^0$	,	$\mathbf{\Phi}_r^\kappa(x)$	=	$\Phi_l^\kappa(x)\mathbf{T}_{lr}$	
$[3 \times 1]$		$[3 \times 1]$	$[3 \times 2][2 \times 1]$	$[3 \times 1]$		$[3 \times 12][12 \times 1]$		$[3 \times 2]$		$[3 \times 12][12 \times 2]$	

Table 7. Natural frequencies of the controlled 24^{th} order model using the controller designed on a 12^{th} order model.

Mode		Controlled Frequencies		Aeroelastic Frequencies	
		frequency (rad/s)	damping	frequency (rad/s)	damping
1^{st}	bending	61.4702	$+8.49722 \cdot 10^{-1}$	69.4195	$+3.26373 \cdot 10^{-1}$
2^{nd}	bending	166.798	$+5.57226 \cdot 10^{-1}$	196.286	$+9.35641 \cdot 10^{-2}$
3^{rd}	bending	376.733	$+1.87119 \cdot 10^{-1}$	375.224	$+4.30848 \cdot 10^{-2}$
1^{st}	lead-lag	68.5258	$+9.22514 \cdot 10^{-1}$	76.2633	$+9.82787 \cdot 10^{-4}$
2^{nd}	lead-lag	452.930	$+5.77833 \cdot 10^{-1}$	455.697	$+1.20758 \cdot 10^{-4}$
1^{st}	torsion	593.846	$+6.24244 \cdot 10^{-1}$	340.945	$+7.47685 \cdot 10^{-2}$

List of Figures

List of Tables